incubation periods of animals cerebrally infected with prion diseases in a prion strain-dependent manner, J. Virol. 81 (2007) 12889–12898.
[12] K. Ishikawa, K. Doh-ura, Y. Kudo, N. Nishida, I. Murakami-Kubo, Y. Ando, T. Sawada, T. Iwaki, Amyloid imaging probes are useful for detection of prion plaques and treatment of transmissible spongiform encephalopathies, J. Gen. Virol. 85 (2004) 1785–1790.
[13] K. Teruya, K. Nishizawa, K. Doh-ura, Semisynthesis of a protein with cholesterol at the C-terminal, targeted to the cell membrane of live cells, Protein J. 29 (2010) 493–500.
[14] M. Fischer, T. Rülicke, A. Raeber, A. Sailer, M. Moser, B. Oesch, S. Brandner, A. Aguzzi, C. Weissmann, Prion protein (PrP) with amino-proximal deletions restoring susceptibility of PrP knockout mice to scrapie, EMBO J. 15 (1996) 1255–1264.
[15] S. Sarkar, D.C. Rubinsztein, Small molecule enhancers of autophagy for neurodegenerative diseases, Mol. Biosyst. 4 (2008) 895–901.
[16] Y. Aguib, A. Heiseke, S. Gilch, C. Riemer, M. Baier, H.M. Schätzl, A. Ertmer, Autophagy induction by trehalose counteracts cellular prion infection, Autophagy 5 (2009) 361–369.
[17] N. Naslavsky, R. Stein, A. Yanai, G. Friedlander, A. Taraboulos, Characterization of detergent-insoluble complexes containing the cellular prion protein and its scrapie isoforms, J. Biol. Chem. 272 (1997) 6324–6331.
[18] B. Caughey, G.J. Raymond, The scrapie-associated form of PrP is made from a cell surface precursor that is both protease- and phospholipase-sensitive, J. Biol. Chem. 266 (1991) 18217–18223.
[19] M. Vey, S. Pilkuhn, H. Wille, R. Nixon, S.J. DeArmond, E.J. Smart, R.G. Anderson, A. Taraboulos, S.B. Prusiner, Subcellular colocalization of the cellular and scrapie prion proteins in caveolae-like membranous domains, Proc. Natl. Acad. Sci. USA 93 (1996) 14945–14949.
[20] Y. Iwamaru, Y. Shimizu, M. Imamura, Y. Murayama, R. Endo, Y. Tagawa, Y. Ushiki-Kaku, T. Takenouchi, H. Kitani, S. Mohri, T. Yokoyama, H. Okada, Lactoferrin induces cell surface retention of prion protein and inhibits prion accumulation, J. Neurochem. 107 (2008) 636–646.
[21] C.L. Kim, A. Karino, N. Ishiguro, M. Shinagawa, M. Sato, M. Horiuchi, Cell-surface retention of PrPC by anti-PrP antibody prevents protease-resistant PrP formation, J. Gen. Virol. 85 (2004) 3473–3482.
[22] G. Forloni, S. Jussich, T. Awan, L. Colombo, N. Angeretti, L. Girola, I. Bertani, G. Poli, M. Caramelli, M. Grazia Bruzzone, L. Farina, L. Limido, G. Rossi, G. Giaccone, J.W. Ironside, O. Bugiani, M. Salmona, F. Tagliavini, Tetracyclines affect prion infectivity, Proc. Natl. Acad. Sci. USA 99 (2002) 10849–10854.
[23] S.P. Wasser, Medicinal mushrooms as a source of antitumor and immunomodulating polysaccharides, Appl. Microbiol. Biotechnol. 60 (2002) 258–274.
[24] M. Ikuzawa, K. Matsunaga, S. Nishiyama, S. Nakajima, Y. Kobayashi, T. Andoh, A. Kobayashi, M. Ohhara, Y. Ohmura, T. Wada, Y. Chikao, Fate and distribution of an antitumor protein-bound polysaccharide PSK (Krestin), Int. J. Immunopharmacol. 10 (1988) 415–423.
[25] H. Endoh, K. Matsunaga, C. Yoshikumi, Y. Kawai, T. Suzuki, K. Nomoto, Production of antiserum against antitumor protein-bound polysaccharide preparation, PSK (Krestin) and its pharmacological application, Int. J. Immunopharmacol. 10 (1988) 103–109.
[26] S. Sethi, G. Lipford, H. Wagner, H. Kretzschmar, Postexposure prophylaxis against prion disease with a stimulator of innate immunity, Lancet 360 (2002) 229–230.

Protein J (2010) 29:493–500
DOI 10.1007/s10930-010-9278-9

Semisynthesis of a Protein with Cholesterol at the C-Terminal, Targeted to the Cell Membrane of Live Cells

Kenta Teruya · Keiko Nishizawa · Katsumi Doh-ura

Published online: 3 September 2010

Abstract Various proteins are modified post-translationally to localize them at the cell membrane. Among them, hedgehog-family proteins are modified by cholesterol at the C-terminal. In this study, green fluorescent protein (GFP) modified with cholesterol (GFP-Chol) at the C-terminal was prepared semisynthetically and investigated. This semi-synthesis was performed using the following native chemical ligation: GFP-Cα-thioester was prepared using the intein-mediated thioester exchange reaction and was ligated to Cys-NH-diethylene glycol-NHCO-cholesterol in the presence of a detergent. After removal of the detergent, the GFP-Chol was applied to mouse live cells. Confocal laser fluorescent microscopy confirmed localization of GFP-Chol at the cell membrane. The findings suggest that modifying proteins with cholesterol at the C-terminal is useful for targeting the proteins to the cell membrane of live cells.

Keywords Chemical modification · C-terminal · Cholesterol · Cell membrane · Semi-synthesis

Abbreviations

Chol	Cholesterol
CTAB	Cetyl trimethyl ammonium bromide
DEG	Diethylene glycol
F	Fluorescein
FAB	Fast atom bombardment
GFP	Green fluorescent protein
MALDI-TOF	Matrix-assisted laser desorption ionization-time of flight
MESNa	Mercapto ethane sulfonic acid sodium salt
MS	Mass spectrometry
PBS	Phosphate-buffered saline
PCR	Polymerase chain reaction
RP-HPLC	Reversed phase-high performance liquid chromatography
SDS-PAGE	Sodium dodecyl sulfate-polyacrylamide gel electrophoresis
TLC	Thin layer chromatography

Electronic supplementary material The online version of this article (doi:10.1007/s10930-010-9278-9) contains supplementary material, which is available to authorized users.

K. Teruya · K. Nishizawa · K. Doh-ura (✉)
Department of Neurochemistry, Tohoku University Graduate School of Medicine, 2-1 Seiryo-Machi, Aoba-Ku, Sendai, Miyagi 980-8575, Japan
e-mail: doh-ura@med.tohoku.ac.jp

1 Introduction

Most proteins require post-translational modifications to exert their functions in live cells. Modification of proteins with lipophilic molecules is necessary for targeting them to the cell membrane and for making them functional in signal transductions and cell–cell interactions. Hedgehog-family proteins, for example, exert developmental signal transductions over the cells neighboring the source of the signal [10], once modified with cholesterol at the C-terminal.

Targeting exogenous artificial proteins to the cell membrane can be useful for pursuing their functions and their interaction with other molecules expressed on the cell membrane of live cells. Common techniques for introducing proteins into live cells include gene transfection, protein modification by an attachment of intracellular compartment localization signals, and receptor-mediated

protein transport. However, no technique has been established to introduce exogenous artificial proteins into the cell membranes of live cells.

We describe the development of a semi-synthetic model protein with a lipophilic molecule at the C-terminal. It was integrated into the cell membrane of live culture cells when added to the cells exogenously. The semi-synthetic protein was produced using a combination of peptide chemical synthesis and recombinant protein-Cα thioester modification technique [3]. The building blocks were ligated by the native chemical ligation method [1, 4, 6, 11], in which a peptide bond is formed via a thiol exchange reaction and an S–N acyl shift between the thioester of a peptide segment and the N-terminal Cys-residue of another peptide segment in aqueous solution.

2 Materials and Methods

Experimental procedures and data are provided in detail in *Supplementary Information*.

2.1 Cloning of GFP-Intein-Chitin Binding Domain

A DNA fragment corresponding to green fluorescent protein (GFP) was obtained from pQBI-pkg (Wako Chemicals USA Inc., VA, USA) using PCR with the primers 5′-CCGG ATCCGGGGCGCGCAAGA-3′ and 5′-CCGCTCGAGAC CGTGTACAGTTCATCCA-3′. This fragment was digested with *Nhe*I and *Xho*I and was ligated into pTYB1 (New England Biolabs Inc.). The resulting plasmid, pGFP/TYB1, contained a DNA sequence of a fusion protein for GFP, a five amino acid peptide linker (Leu-Glu-Gly-Ser-Ser), and a *Saccharomyces cerevisiae* intein with an affinity tag, the chitin-binding domain, placed at the C-terminal. Using this plasmid as a template, we prepared an insert for another vector pTXB1 (New England Biolabs Inc.) using PCR with the primers 5′-TAATACGACTCACTATAGGG-3′ and 5′-CTTGCTCTTCGGCAACCGTTGTACAGTTCATCCA TG-3′. This insert was digested with *Nhe*I and *Sap*I and was ligated to generate pGFP/TXB1. Plasmid vector pGFP-Met/TXB1—which contained a methionine residue insert between GFP and the intein that was reported as suitable for the production of protein-Cα-thioester [19]—was prepared using site-directed mutagenesis with the primers 5′-CTGTACAACGGTATGTGCATCACGGGA-3′ and 5′-TCCCGTGATGCACATACCGTTGTACAG-3′.

2.2 Preparation of GFP-Cα-Thioester

Fusion proteins of GFP-intein were expressed in *Escherichia coli* BL21 cells. The cell pellets (typically 2.3 g of wet cells from 500 mL of culture) were resuspended in a lysis buffer (20 mM Tris-HCl, 300 mM NaCl, pH 7.5) containing phenylmethylsulfonyl fluoride. The cells were lysed by sonication and were centrifuged. The supernatants were applied to a 5-mL-volume chitin bead column (New England Biolabs Inc.). The column was washed thoroughly in lysis buffer and rocked at 37 °C overnight in the presence of mercapto ethane sulfonic acid sodium salt (MESNa) to produce GFP-Cα-MESNa. The beads were filtered off and rinsed. Aliquots of each step were monitored using SDS-PAGE.

The solution of GFP-Cα-MESNa was concentrated 10-fold using centrifugal dialysis (Amicon Ultra-3; Millipore Corp., MA, USA). The buffer was exchanged to aqueous $NaHCO_3$ (200 mM, pH 8.5). The solution was frozen immediately until use. The procedure gave 1.0 mg of GFP product, as determined by UV absorption at 488 nm, from 500 mL culture. The band on SDS-PAGE corresponding to GFP product was subject to tryptic digestion. Following desalt and condensation with ZipTip C_{18} (Millipore Corp.), the peptides were analyzed using MALDI-TOF MS (Voyager STR; Applied Biosystems, CA, USA) using α-cyano-4-hydroxyciannamic acid as a matrix. The analysis revealed peptide fragments corresponding to 5–27, 28–42, 47–53, 81–86, 87–102, 115–127, 133–141, 142–157, and 216–240 of GFP (data not shown). The purity and molecular weight were checked using SDS-PAGE.

2.3 Synthesis of NH_2-DEG-NHCO-Chol and Cys-NH-DEG-NHCO-Chol

Cholesterol chloroformate was condensed with an excess molar amount of 4,7,10-trioxa-1,13-tridecane diamine (NH_2-DEG-NH_2). After 60 min incubation, the reaction mixture was washed with water. Then the reaction mixture was applied to a silica column and eluted. The fractions containing NH_2-DEG-NHCO-Chol were combined and evaporated. The coupling product was analyzed using TLC. FAB-MS, 633.5202 (theoretical $[M + H]^+ = 633.5206$).

In the presence of *N*,*N*-diisopropylethylamine, NH_2-DEG-NHCO-Chol was reacted with *N*-(*N*-α-trityl-*S*-trityl-L-cysteinyloxy)succinimide. After 60 min, the product was purified on a silica column. A protecting group of the product was removed through treatment with trifluoroacetic acid and triisopropylsilane. The product Cys-NH-DEG-NHCO-Chol was purified using a silica column. The fractions containing Cys-NH-DEG-NHCO-Chol were combined and evaporated. The residue was suspended in water and frozen until use. FAB-MS, 758.5122 (theoretical $[M + Na]^+ = 758.5118$).

2.4 Synthesis of F-NH-DEG-NH_2 and F-NH-DEG-NHCO-Chol

Succimidyl ester of 5-carboxyfluorescein (F) was reacted with NH_2-DEG-NH_2 or NH_2-DEG-NHCO-Chol. After 60 min of incubation, the product was purified using a silica column. After evaporation, the residue was dissolved in water. The quantity was estimated using UV measurement. FAB-MS was 579.2347 (theoretical $[M + H]^+ = 579.2343$) for F-NH-DEG-NH_2 and 1013.5507 (theoretical $[M + Na]^+ = 1013.5503$) for F-NH-DEG-NHCO-Chol, respectively.

2.5 Synthesis of Cys-Lanthanide Binding Peptide

Starting from Fmoc-Gly Wang resin, FIDTNNDGWIEGDELLLEEGG-resin was synthesized using a peptide synthesizer (ABI 433A; Applied Biosystems) with 2-(1H-benzotriazole-1-yl)-1,1,3,3-tetramethyluronium hexafluorophosphate as a coupling reagent. To this peptide resin, tBoc-Cys(Trt) was incorporated manually. Crude peptide was obtained using a cleavage reaction. It was subject to RP-HPLC purification. MALDI-TOF MS was 2440.58 (theoretical $[M + H]^+ = 2440.31$).

2.6 Native Chemical Ligation of GFP-Cα-MESNa with Cys-Derivatives

The solution of GFP-Cα-MESNa was condensed with Cys-lanthanide binding peptide, Cys-NH-DEG-NHCO-Chol, or 1,4-dithio-DL-threitol (DTT) in the presence of $NaHCO_3$, tris(hydroxypropyl)phosphine and cetyl trimethyl ammonium bromide (CTAB). The coupling mixture was incubated for 24 h at room temperature under nitrogen. The reaction buffer was exchanged to PBS repeatedly by ultracentrifugation. The GFP product concentration was determined using UV measurement. The progress of the coupling reaction was monitored using SDS-PAGE.

An aliquot of the coupling reaction mixture between GFP-Cα-MESNa and Cys-NH-DEG-NHCO-Chol was subject to chloroform–methanol protein precipitation to remove salts and detergents from the mixture. The precipitated protein was analyzed using RP-HPLC (LC10A; Shimadzu Corp., Kyoto, Japan) with a C_4 column ($5C_4$-AR300; 4.6 × 150 mm, Nacalai Tesque Inc., Kyoto, Japan). Results of MALDI-TOF MS were 26857.9 corresponding to GFP (theoretical $[M + H]^+ = 26997.9$), and 27571.1 corresponding to GFP-Chol (theoretical $[M + H]^+ = 27716.9$). A difference of 140 Da was found between the observed mass number and the calculated mass number of both unmodified and modified GFP. This result might be attributed to degradation of the first methionine residue, causing a 131 Da decrease in the mass number.

2.7 Fluorescence Microscopy

Cultured N2a cells in Opti-MEM (Invitrogen Corp. CA, USA), supplemented with 10% fetal calf serum on a glass-bottom dish, were rinsed three times with cold PBS. Each sample of modified GFP (final conc. 4.8 μM), unmodified GFP (final conc. 4.8 μM), F-NH_2 (final conc. 0.84 μM) and F-Chol (final conc. 1.2 μM) was added to the cells in cold PBS. For double staining, both modified GFP (final conc. 4.8 μM) and rhodamine-labeled 3F4 anti-prion protein antibody (final conc. ca. 1.2 μg/mL) were added to the cells in cold PBS. After 15 min incubation under a cold condition, the cells were rinsed with cold PBS. Then the cells were observed using confocal fluorescence microscopy (magnification ×60) (Fluoview FV300; Olympus Corp., Tokyo). Prion protein, a glycosyl phosphatidyl inositol-anchored protein, was used as a marker protein for the lipid raft microdomain of the cell membrane.

2.8 Density Gradient Fractionation Analysis

Density gradient fractionation analysis of the cell membrane components was performed as described by Naslavsky and colleagues [12]. Briefly, cells that had been grown confluently in two flasks (25 cm^2) were labeled with GFP-Chol or F-Chol as described above. Then the cells were lysed with 500 μL of lysis buffer (150 mM NaCl, 25 mM Tris–HCl, pH 7.5, 5 mM ETDA, 1% Triton X-100) on ice for 30 min. The lysate (400 μL) was mixed with an equal volume of ice-cold 70% Nycodenz prepared in TNE (25 mM Tris, pH 7.5, 150 mM NaCl, 5 mM EDTA) and loaded to an ultracentrifuge tube. Then the lysate was overlaid sequentially with 200 μL each of 25, 22.5, 20, 18, 15, 12, and 8% Nycodenz in TNE. The tube was spun at 200,000×g for 4 h at 4 °C using a micro-ultracentrifuge (CS 120 GX; Hitachi Ltd., Tokyo, Japan). Eleven fractions containing 200 μL each were collected from the top of the tube.

An aliquot of each fraction was subject to fluorescence analysis and immunoblotting. Fluorescence was analyzed using a microplate reader (ARVO, MX; PerkinElmer Inc., MA, USA) to detect GFP-Chol and F-Chol. For immunoblotting detection of GFP-Chol, we used mouse monoclonal anti-GFP antibody (ab1218; Abcam plc., MA, USA) as a primary antibody and rabbit anti-mouse IgG as a secondary antibody.

3 Results and Discussion

We used GFP as a model protein because of its easy traceability. Then we modified it by introducing a cholesterol (Chol) group at the C-terminal to target it to the cell

membrane of live cells. The modified GFP was produced using a combination of recombinant protein synthesis in *E. coli* and chemical synthesis.

3.1 Semi-Synthesis of GFP-Cys-NH-DEG-NHCO-Chol (GFP-Chol)

Semi-synthesis of GFP-Cys-NH-DEG-NHCO-Chol (GFP-Chol) was achieved by condensation of building blocks corresponding to GFP and Chol. The building block for GFP consisted of a GFP bearing a modification moiety. The building block for Chol consisted of Chol and a hydrophilic linker with Cys at the terminal (Fig. 1). The building block for GFP was prepared using *E. coli* recombinant protein expression; the building block for Chol was prepared using chemical synthesis. Then both building blocks were condensed using the native chemical ligation method [6] under an aqueous condition. Similar semi-synthetic strategies have been described in previous reports [5, 13–15].

The GFP-Cα-thioester was prepared by application of intein-mediated thiolysis to a GFP-intein fusion recombinant protein (Fig. 1a). To produce the recombinant protein, three constructs were examined: (1) a GFP DNA fragment was inserted into the *NheI*/*XhoI* site of pTYB1 vector (New England Biolabs Inc., MA, USA), (2) a DNA fragment was inserted into the *NheI*/*SapI* site of pTXB1 vector (New England Biolabs Inc.), and (3) a DNA fragment of GFP plus a methionine residue between GFP and intein was inserted into the *NheI*/*SapI* site of pTXB1 vector; the last construct was examined because methionine is reportedly a suitable amino acid residue for the production of protein-Cα-thioester [19]. Among them, the second construct—GFP DNA fragment inserted into the *NheI*/*SapI* site of pTXB1—produced a suitable fusion recombinant protein that was then cleaved into GFP-Cα-thioester by intein-mediated thiolysis. The cleavage reaction was controlled by MESNa added to the recombinant protein solution; the GFP-Cα-thioester product was recovered as presented in Figure S10B. On the other hand, the first construct produced a recombinant protein from which no cleavage product was obtained. The third construct produced a recombinant protein that was cleaved into products having no Cα-thioester, even in the absence of MESNa and even at 4 °C.

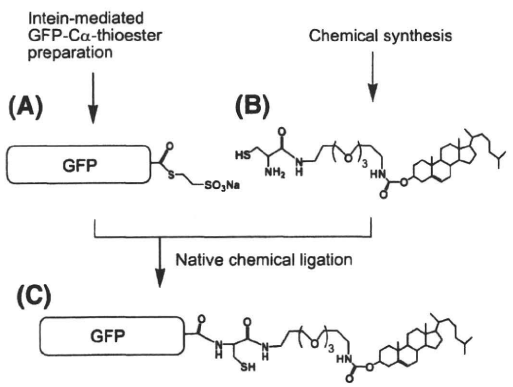

Fig. 1 Schematic representation of semisynthesis of cholesterol-modified GFP. **a** GFP-Cα-thioester preparation by intein-mediated thiolysis. **b** Synthetic scheme of the amphitropic part. The Cys residue was incorporated for the subsequent condensation reaction. Intermediates were used for the synthesis of control compounds. **c** Modification by the native chemical ligation method. The thiol exchange reaction was followed by an S–N acyl shift to generate a peptide bond

The building block for Chol (Fig. 1b) was synthesized with Chol, a hydrophilic diethylene glycol-based diamine linker (NH_2-DEG-NH_2), and a chemoselective reaction moiety to the Cα-thioester, Cys [6]. These three chemical components were condensed sequentially. Briefly, NH_2-DEG-NH_2 was reacted with Chol chloroformate. After NH_2-DEG-NHCO-Chol was isolated using a silica column, a Cys residue was incorporated at the other amino group. After deprotection and isolation, Cys-NH-DEG-NHCO-Chol was obtained. These coupling reactions and products were confirmed using TLC and FAB-MS.

The building blocks for GFP and Chol were condensed using the native chemical ligation method. The ligation reaction was performed in the presence of 20 mM of CTAB to solubilize the amphitropic unit of the building block for Chol during the ligation [7]. The product from the reaction of GFP-Cα-thioester with Cys-NH-DEG-NHCO-Chol showed no obvious mobility difference on SDS–PAGE from that of the reaction of GFP-Cα-thioester with DTT (Fig. 2, lanes 2 and 4). Therefore, we tested whether the ligation conditions and GFP-Cα-thioester were suitable for reaction by monitoring the ligation of GFP-Cα-thioester with the Cys-lanthanide binding peptide composed of 21 amino acid residues [8] (Fig. 2, lane 3). The product of this ligation showed a mobility shift. Its yield was estimated as approximately 50% of the initial material on SDS-PAGE. Therefore, we presumed that the ligation conditions and GFP-Cα-thioester were suitable for the reaction.

After both the detergent and the Cys-NH-DEG-NHCO-Chol were removed using chloroform–methanol precipitation, the ligation product was separated from unligated GFP-Cα-thioester by RP-HPLC column (Fig. 3a). In the elution profile, a peak corresponding to GFP-Cα-thioester [RT 26 min (*) in Fig. 3a] was followed by a new peak [RT 36 min (**) in Fig. 3a], indicating that the hydrophobicity of the ligation product was increased significantly. The yield of the ligation product was estimated as 45% of the initial material and was almost comparable to that of the ligation product with the Cys-lanthanide

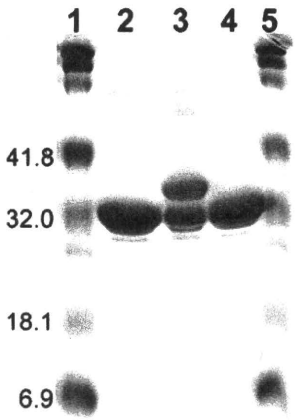

Fig. 2 Coupling reaction of GFP-Cα-thioester with Cys-derivatives. Coomassie-stained SDS-PAGE of the products from GFP-Cα-thioester reacted with DTT (*lane 2*), Cys-lanthanide binding peptide (*lane 3*) and Cys-NH-DEG-NHCO-Chol (*lane 4*) is shown. The molecular weight marker (kDa units) is included in *lanes 1* and *5*. The coupling reaction proceeded successfully in *lane 3*. No significant mobility change was observed in *lane 2* or *4*

binding peptide. Subsequent MALDI-TOF MS analysis of the material from each peak revealed that the ligation product was GFP-Chol. The mass number difference between the materials at each peak was 713 Da (Fig. 3b), which was almost identical to the calculated value of 719 Da. These results indicated that the semisynthesis was successfully performed.

3.2 Synthesis of Fluorescein-NH-DEG-NHCO-Chol (F-Chol)

Fluorescein-labeled Chol (F-Chol) was prepared by condensing fluorescein and NH_2-DEG-NHCO-Chol. Actually, F-Chol acted as a control to evaluate the Chol function. The ligation product was water-soluble and separated as described for GFP-Chol. The separation method did not affect the fluorescence function of F-Chol. Sato and colleagues reported the synthesis and application of a fluorescein ester of polyethylene glycol-modified cholesterol which labeled cholesterol-rich membranes in both live cells and in model membranes [17]. Compared to their compound, F-Chol is simpler and more stoichiometrically homogeneous. The orientation of Chol within the plasma membrane may differ dramatically according to the modification site in Chol scaffold [18]. Hedgehog proteins are modified by an ester formation between the C-terminal of the protein and the secondary alcohol of Chol [10]. Taking these into account, we decided to use the secondary alcohol group in Chol as the ligation site in the present study.

3.3 Application to Mouse Neuroblastoma N2a Cells

The GFP-Chol separation method described above, which included two protein denaturing steps, caused such denaturation of GFP-Chol that no attempt was able to refold it to an active fluorescence form. Therefore, the reaction mixture containing both GFP-Chol and GFP was used for

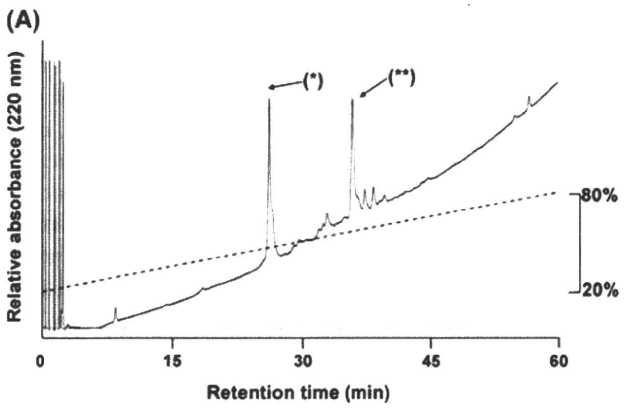

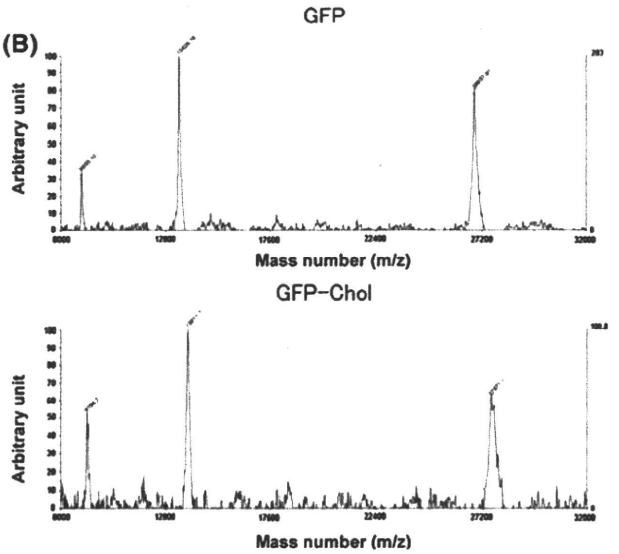

Fig. 3 Analysis of coupling reaction products. **a** RP-HPLC profile of the crude mixture after coupling reaction. The peaks *arrowed* by (*) and (**), respectively correspond to GFP and GFP-Chol. **b** MALDI-TOF MS data for GFP and GFP-Chol. Observed mass numbers for GFP and GFP-Chol were 26857.9 (theoretical $[M + H]^+ = 26997.9$) and 27571.1 (theoretical $[M + H]^+ = 27716.9$), respectively, indicating a 713 increase in mass number after Chol-modification

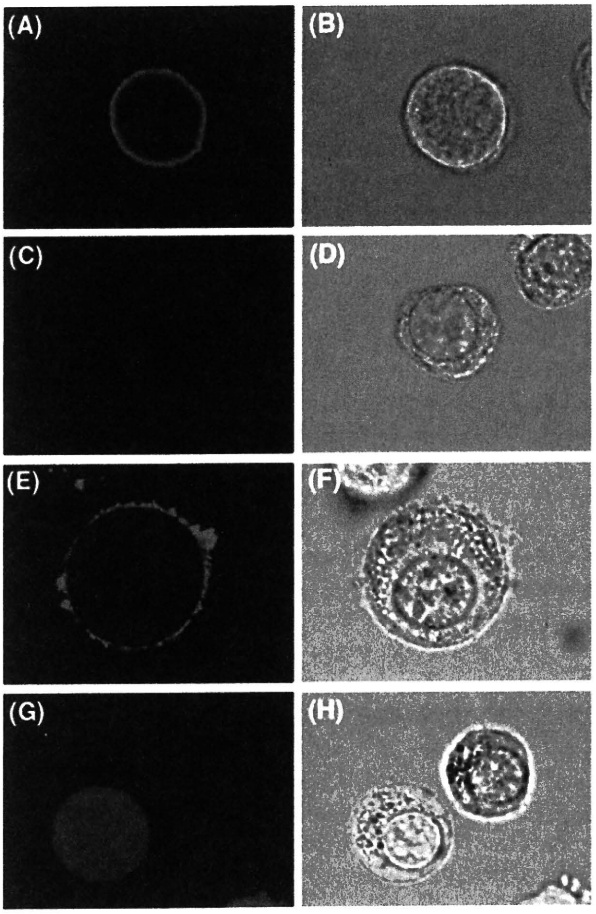

Fig. 4 Fluorescence microscopy images of GFP-Chol and control compounds in N2a cells. N2a cells were observed by confocal laser fluorescence microscopy after incubation with GFP-Chol (**a** and **b**), GFP (**c** and **d**), F-Chol (**e** and **f**) and F-NH_2 (**g** and **h**). Fluorescence images (**a**, **c**, **e** and **g**) were merged with corresponding differential interference contrast images (**b**, **d**, **f** and **h**). Fluorescence signals were observed at the cell membrane in GFP-Chol and F-Chol, but not in GFP and F-NH_2

application to live cells after extensive ultrafiltration with PBS to remove detergents. The results of this mixture sample were then compared to those of the sample containing GFP alone. The content of GFP-Chol in the mixture sample was estimated as 45% by RP-HPLC analysis (Fig. 3a). No significant difference in the fluorescence spectra were observed between the two samples (Figure S11). The GFP moiety concentration was determined by absorption at 488 nm wavelength.

The mouse neuroblastoma N2a cells were incubated with the samples at 4 °C for 15 min. Confocal fluorescent microscopy analysis revealed that the GFP-Chol was retained homogenously at the cell membrane (Fig. 4a, b), although GFP prepared by hydrolysis of GFP-Cα-thioester was rinsed off with cold PBS (Fig. 4c, d). The homogenous retention of GFP-Chol at the cell membrane was observed

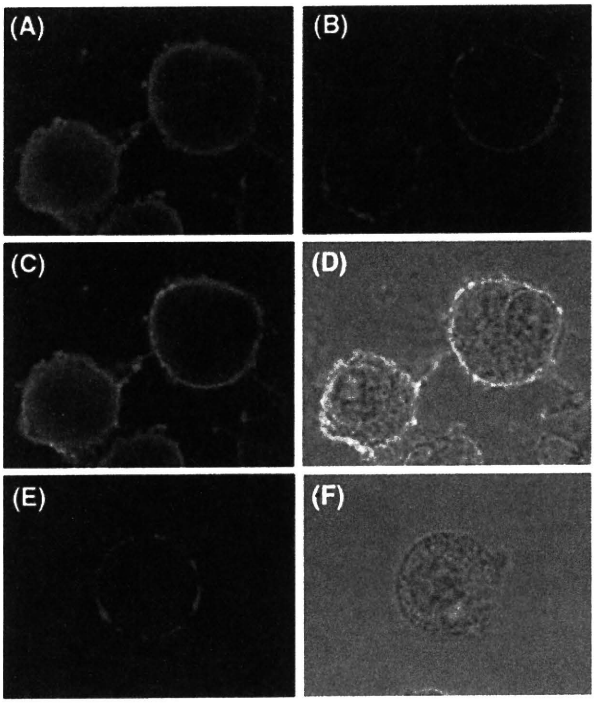

Fig. 5 Fluorescence microscopy images for GFP-Chol and prion protein in N2a cells. N2a cells were observed by confocal laser fluorescence microscopy after incubation with GFP-Chol and rhodamine-labeled anti-prion protein antibody. Fluorescence image for GFP-Chol (**a**) and for prion protein (**b**) were merged without the differential interference contrast image (**c**) or with the contrast image (**d**). The signals for GFP-Chol were rather homogenously distributed at the cell membrane as demonstrated in Fig. 4a, but those for prion protein were distributed in a patchy pattern at the cell membrane. This prion protein distribution pattern at the cell membrane was similarly observed in the cells incubated with only rhodamine-labeled anti-prion protein antibody (**e** and **f**)

also in live cells of other types, such as mouse bone marrow-derived mast cells (data not shown).

To clarify the function of Chol itself, F-Chol and F-NH_2 were also applied to the N2a cells. In fact, F-Chol was observed at the cell membrane (Fig. 4e, f). However, most of F-NH_2 was rinsed off, and a small portion was observed inside of the cells (Fig. 4g, h). The internalization of F-NH_2 might have been caused by the passive intake of an amino moiety [9], which was included in F-NH_2 but not in F-Chol. These findings suggest that Chol modification allows molecules to be targeted to the cell membrane.

To compare the distribution of GFP-Chol with that of a lipid raft marker protein in the N2a cells, we performed double staining for GFP-Chol and prion protein, a glycosyl phosphatidyl inositol-anchored protein known to localize in the lipid raft microdomain of the cell membrane [12, 20]. The signals for GFP-Chol were rather homogenously distributed at the cell membrane (Fig. 5a) as already shown in Fig. 4a. However, the signals for prion protein were distributed in a patchy pattern at the cell membrane (Fig. 5b)

and did not necessarily co-localize with the signals for GFP-Chol (Fig. 5c, d). We confirmed that the GFP-Chol treatment of the cells did not affect the distribution pattern of prion protein at the cell membrane, by comparing the prion protein images of GFP-Chol-treated N2a cells (Fig. 5b) with those of untreated N2a cells (Fig. 5e, f).

3.4 Distribution of GFP-Chol and F-Chol at the Cell Membrane

To investigate the distribution of GFP-Chol and F-Chol at the cell membrane of N2a cells, density gradient fractionation of the cell membrane components [2] was performed. Each fraction was analyzed using detection of fluorescence (Fig. 6a). We detected both GFP-Chol and F-Chol in the high-density fractions of the cell membrane. Immunoblot analysis of GFP from an aliquot of each fraction confirmed the results of the fluorescence analysis (Fig. 6b). In contrast to GFP-Chol and F-Chol, prion protein is known to distribute in the low-density fractions of the cell membrane in N2a cells [12], as demonstrated in Figure S13.

The results of either confocal laser fluorescent microscopy analysis or density gradient fractionation analysis are apparently different from those of previous studies, where proteins fused with a signal peptide for post-translational lipid-modification were expressed in the lipid raft microdomain [10, 16, 21], or where an exogenously added Chol-modified fluorescein was observed in the lipid raft microdomain [17]. This difference might be caused by our method of Chol-modification, because modified Chol may have different orientations from that of native Chol within the plasma membrane [18]. Also, it is presumable that the difference might be attributable to variations in such materials used in the experiments as cell types, modified protein types, and stoichiometry of Chol in tested molecules. In addition, it is conceivable that exposure of relatively high concentrations of our Chol-modified molecules to live cells might alter selective incorporation of the molecules into proper portions of the cell membrane or might disturb the cell membrane integrity. However, all these possibilities remain to be further evaluated.

In conventional chemical modifications of proteins, chemical reactions tend to occur more efficiently on the protein surface, where epitopes or functional groups of the proteins can be damaged. Therefore, proteins must be modified in such a fashion that their functional groups can be maintained properly. The present study demonstrated a specific chemical modification of a model protein to deliver it to the cell membrane of live cells without damaging the protein's functional activity. This kind of specific chemical modification of proteins is a key requirement for applying the proteins in in vivo or ex-vivo systems.

4 Conclusion

We demonstrated the semisynthesis of GFP specifically modified with Chol at the C-terminal. Results show that the

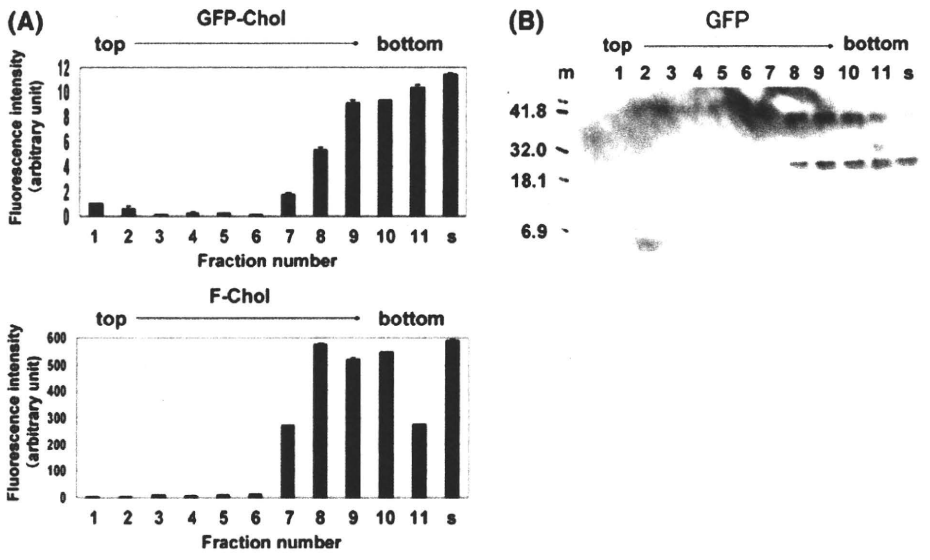

Fig. 6 Density gradient fractionation data of GFP-Chol and F-Chol in N2a cells. N2a cells incubated with GFP-Chol or F-Chol were lysed under a mild condition. The lysate was fractionated. Numbering order is from the top fraction (low density) to the bottom fraction (high density) in an 8–35% linear density gradient. The starting material before fractionation is indicated as "s". **a** Fluorescence data for GFP-Chol and F-Chol. Both fluorescence signals were distributed in higher density fractions. **b** Immunoblotting data for GFP. Signal distribution pattern for GFP was consistent with that of GFP-Chol fluorescence. The molecular weight marker in the left "m" is shown in kDa units

protein remained functional and was localized at the cell membrane, when added to live cells exogenously. These findings suggest that modifying proteins with Chol at the C-terminal is useful for targeting proteins to the cell membrane of live cells.

Acknowledgments This research was supported by Grants-in-Aid for Scientific Research No. 16750138 and No. 18750139 from the Ministry of Education, Culture, Sports, Science and Technology, Japan and by a grant from the Ministry of Health, Labour, and Welfare. MALDI-TOF MS data were obtained with the support of Biomedical Research Core of Tohoku University Graduate School of Medicine. The FAB-MS data used in this study were obtained with the assistance of Prof. Akaji, Kyoto Prefecture Medical University. This work was partly performed under the Cooperative Research Program of Institute for Protein Research, Osaka University.

References

1. Aimoto S (2001) Curr Org Chem 5:45–87
2. Brown DA, Rose JK (1992) Cell 68:533–544
3. Chong S, Shao Y, Paulus H, Benner J, Perler FB, Xu MQ (1996) J Biol Chem 271:22159–22168
4. David R, Richter MP, Beck-Sickinger AG (2004) Eur J Biochem 271:663–677
5. Dawson PE, Kent SB (2000) Annu Rev Biochem 69:923–960
6. Dawson PE, Muir TW, Clark-Lewis I, Kent SB (1994) Science 266:776–779
7. Durek T, Alexandrov K, Goody RS, Hildebrand A, Heinemann I, Waldmann H (2004) J Am Chem Soc 126:16368–16378
8. Franz KJ, Nitz M, Imperiali B (2003) Chembiochem 4:265–271
9. Guy-Caffey JK, Bodepudi V, Bishop JS, Jayaraman K, Chaudhary N (1995) J Biol Chem 270:31391–31396
10. Jeong J, McMahon AP (2002) J Clin Invest 110:591–596
11. Muir TW, Sondhi D, Cole PA (1998) Proc Natl Acad Sci USA 95:6705–6710
12. Naslavsky N, Stein R, Yanai A, Friedlander G, Taraboulos A (1997) J Biol Chem 272:6324–6331
13. Olschewski D, Seidel R, Miesbauer M, Rambold AS, Oesterhelt D, Winklhofer KF, Tatzelt J, Engelhard M, Becker CF (2007) Chem Biol 14:994–1006
14. Paulick MG, Wise AR, Forstner MB, Groves JT, Bertozzi CR (2007) J Am Chem Soc 129:11543–11550
15. Pellois JP, Muir TW (2005) Angew Chem Int Ed Engl 44:5713–5717
16. Rietveld A, Neutz S, Simons K, Eaton S (1999) J Biol Chem 274:12049–12054
17. Sato SB, Ishii K, Makino A, Iwabuchi K, Yamaji-Hasegawa A, Senoh Y, Nagaoka I, Sakuraba H, Kobayashi T (2004) J Biol Chem 279:23790–23796
18. Scheidt HA, Muller P, Herrmann A, Huster D (2003) J Biol Chem 278:45563–45569
19. Southworth MW, Amaya K, Evans TC, Xu MQ, Perler FB (1999) Biotechniques 116:118–120
20. Stahl N, Borchelt DR, Hsiao K, Prusiner SB (1987) Cell 51:229–240
21. Vincent S, Thomas A, Brasher B, Benson JD (2003) Nat Biotechnol 8:936–940

Eur J Nucl Med Mol Imaging (2010) 37:934–941
DOI 10.1007/s00259-009-1314-7

ORIGINAL ARTICLE

In vivo detection of prion amyloid plaques using [^{11}C]BF-227 PET

Nobuyuki Okamura · Yusei Shiga · Shozo Furumoto · Manabu Tashiro · Yoshio Tsuboi · Katsutoshi Furukawa · Kazuhiko Yanai · Ren Iwata · Hiroyuki Arai · Yukitsuka Kudo · Yasuhito Itoyama · Katsumi Doh-ura

Received: 7 August 2009 / Accepted: 21 October 2009 / Published online: 17 December 2009

Abstract
Purpose In vivo detection of pathological prion protein (PrP) in the brain is potentially useful for the diagnosis of transmissible spongiform encephalopathies (TSEs). However, there are no non-invasive ante-mortem means for detection of pathological PrP deposition in the brain. The purpose of this study is to evaluate the amyloid imaging tracer BF-227 with positron emission tomography (PET) for the non-invasive detection of PrP amyloid in the brain.
Methods The binding ability of BF-227 to PrP amyloid was investigated using autoradiography and fluorescence microscopy. Five patients with TSEs, including three patients with Gerstmann-Sträussler-Scheinker disease (GSS) and two patients with sporadic Creutzfeldt-Jakob disease (CJD), underwent [^{11}C]BF-227 PET scans. Results were compared with data from 10 normal controls and 17 patients with Alzheimer's disease (AD). The regional to pons standardized uptake value ratio was calculated as an index of BF-227 retention.
Results Binding of BF-227 to PrP plaques was confirmed using brain samples from autopsy-confirmed GSS cases. In clinical PET study, significantly higher retention of BF-227 was detected in the cerebellum, thalamus and lateral temporal cortex of GSS patients compared to that in the corresponding tissues of normal controls. GSS patients also showed higher retention of BF-227 in the cerebellum, thalamus and medial temporal cortex compared to AD patients. In contrast, the two CJD patients showed no obvious retention of BF-227 in the brain.
Conclusion Although [^{11}C]BF-227 is a non-specific imaging marker of cerebral amyloidosis, it is useful for in vivo detection of PrP plaques in the human brain in GSS, based on the regional distribution of the tracer. PET amyloid imaging might provide a means for both early diagnosis and non-invasive disease monitoring of certain forms of TSEs.

N. Okamura · S. Furumoto · K. Yanai
Department of Pharmacology,
Tohoku University School of Medicine,
Sendai, Japan

Y. Shiga · Y. Itoyama
Department of Neurology,
Tohoku University School of Medicine,
Sendai, Japan

S. Furumoto · R. Iwata
Division of Radiopharmaceutical Chemistry,
Cyclotron and Radioisotope Center, Tohoku University,
Sendai, Japan

M. Tashiro
Division of Cyclotron Nuclear Medicine,
Cyclotron and Radioisotope Center, Tohoku University,
Sendai, Japan

Y. Tsuboi
Department of Neurology,
Fukuoka University School of Medicine,
Fukuoka, Japan

K. Furukawa · H. Arai
Department of Geriatrics and Gerontology,
Division of Brain Sciences, Institute of Development,
Aging, and Cancer, Tohoku University,
Sendai, Japan

Y. Kudo
Innovation of New Biomedical Engineering Center,
Tohoku University,
Sendai, Japan

K. Doh-ura (✉)
Department of Prion Research,
Tohoku University School of Medicine,
2-1 Seiryo-machi, Aoba-ku, Sendai 980-8575, Japan
e-mail: doh-ura@mail.tains.tohoku.ac.jp

Keywords Prion · PET · Amyloid · Creutzfeldt-Jakob disease

Introduction

Transmissible spongiform encephalopathies (TSEs), also known as prion diseases, are a group of fatal neurodegenerative disorders, including Creutzfeldt-Jakob disease (CJD), Gerstmann-Sträussler-Scheinker disease (GSS) and kuru [1–3]. TSEs are characterized by progressive deposition of abnormal prion protein (PrP) in the brain. CJD is the most common type of human TSE and is classified into sporadic, genetic and infectious forms according to the aetiology of illness. GSS is a familial neurodegenerative disorder associated with mutations of the PrP gene and is clinically recognized by cerebellar ataxia combined with postural abnormalities and cognitive decline [1–3]. Two major types of abnormal PrP deposition, synaptic and plaque types, have been described in the brain of people with TSEs [1]. The synaptic type of PrP deposition, which does not have tinctorial properties of amyloid in tissue sections, is most commonly observed in sporadic CJD, whereas the plaque type, which frequently forms congophilic amyloid plaques, is a hallmark of such TSEs as GSS, variant CJD (vCJD) and iatrogenic dura CJD with plaques [1, 4]. Abnormal PrP deposition in the brain is suggested to start before the occurrence of clinical symptoms [5–7]. Thus, preclinical diagnosis and, when available, early disease-specific therapeutic interventions, can be beneficial for people predisposed to or affected by TSEs.

Several positron emission tomography (PET) imaging agents have been recently developed and used for in vivo detection of brain amyloid-β (Aβ) plaques in patients with Alzheimer's disease (AD) [8–12]. Most of these β-sheet binding agents show high binding affinity to PrP amyloid because PrP aggregates in TSEs form β-pleated sheet structures and share a common secondary structure with Aβ deposits in AD brains [13–16]. Therefore, these agents would be useful for the in vivo detection of PrP amyloid in the brain. Two clinical PET studies were performed using [^{18}F]FDDNP and/or [^{11}C]PIB in sporadic and familial CJD patients [17, 18]. The results indicated moderate retention of FDDNP and no obvious retention of PIB in the brain [17, 18]. Therefore, agents that can sensitively detect abnormal PrP deposits should be further explored for the diagnosis of TSEs. We have demonstrated in vitro and in vivo binding of benzoxazole derivatives to both Aβ and PrP amyloids [19, 20]. One of these derivatives, BF-227, was used for a clinical PET study where it successfully visualized amyloid deposits in the brain of AD patients in vivo [12, 21]. Therefore, [^{11}C]BF-227 appears to be a promising candidate for PET imaging of PrP deposits. The purpose of this study was to evaluate the clinical utility of [^{11}C]BF-227 PET for the non-invasive detection of abnormal PrP deposits in patients with TSEs.

Methods

Preparation of compounds

BF-227 and its 2-tosyloxyethoxy and *N*-desmethylated derivatives were custom synthesized by Tanabe R&D Service Co. (Osaka, Japan). [^{18}F]BF-227 was synthesized for autoradiography of brain sections, as described previously [22]. For the clinical studies, [^{11}C]BF-227 was synthesized as described previously [12]. Radiochemical yields were greater than 50% based on [^{11}C]methyl triflate, and specific radioactivities were 119–138 GBq/μmol at the end of synthesis. Radiochemical purities were greater than 95%.

Histopathological staining and in vitro autoradiography

Autopsy-diagnosed brain samples from two GSS cases with PrP plaque deposition and two sporadic CJD cases with synaptic PrP deposition were provided by Dr. Toru Iwaki of the Department of Neuropathology, Kyushu University, Japan. The brain sample from an 81-year-old man with autopsy-confirmed physiological aging was obtained from Tohoku University Hospital. The two GSS cases had a proline-to-leucine mutation at codon 102 and methionine homozygosity at codon 129 of the PrP gene, and the two sporadic CJD cases had no mutations and methionine homozygosity at codon 129; they showed type 1 abnormal PrP in immunoblotting of the brain tissues. All of the brain samples were treated with 98% formic acid for 1 h before paraffin embedding to eliminate prion infectivity. Sections from paraffin-embedded blocks of the cerebellum or frontal cortex were then dewaxed in xylene and ethanol. For staining with BF-227, tissue sections were immersed in 100 μM BF-227 solution containing 50% ethanol for 10 min. They were then dipped briefly into water and rinsed in phosphate-buffered saline for 10 min before coverslipping with FluorSave Reagent (Calbiochem, La Jolla, CA, USA). Subsequently, they were examined using an Eclipse E800 microscope (Nikon, Tokyo, Japan) equipped with a V-2A filter set (excitation, 380–420 nm; dichroic mirror, 430 nm; Longpass filter, 450 nm). For autoradiography, the section was incubated with 1.0 MBq/ml of [^{18}F]BF-227 at room temperature for 10 min and then washed briefly with water and 50% ethanol. After drying, the labelled section was exposed to a BAS-III imaging plate (Fuji Film, Tokyo, Japan) overnight. Autoradiographic images were obtained using a BAS-5000 phosphor imaging instrument (Fuji Film, Tokyo, Japan). Neighbouring sec-

tions were immunostained using 3F4 anti-PrP monoclonal antibody (Covance, Princeton, NJ, USA) as described previously [13, 20].

Subjects and patients in the clinical PET study

Five TSE patients, including two sporadic CJD patients [63-year-old woman (CJD1) and 58-year-old man (CJD2)] and three GSS patients [69-year-old woman (GSS1), 61-year-old man (GSS2) and 30-year-old woman (GSS3)], underwent PET scans with [^{11}C]BF-227 (Table 1). For comparison, [^{11}C]BF-227 PET studies were also performed in 17 AD patients [mean age ± standard deviation (SD)= 72.6±6.7; mean Mini-Mental State Examination score ± SD=19.8±4.0] and 10 aged normal controls (mean age ± SD=67.2±2.5). Some of these AD and normal subjects were included in our previous report [12].

CJD1's health was unremarkable until the manifestation of depressive symptoms at the age of 62 years. The patient then developed subacutely progressive dementia, motor disturbances and myoclonus. CJD2 showed subacutely progressive dementia and gait disturbance and then developed psychotic symptoms, dysarthria and myoclonus. Both CJD patients had no mutations and showed methionine homozygosity at codon 129 of the PrP gene. PET studies in CJD1 and CJD2 were performed when they reached grade 4 of the modified Rankin scale at 3 and 4 months after onset of symptoms, respectively. Both patients showed periodic synchronous discharges in electroencephalograms and hyperintensity in the caudate, putamen and cerebral cortex on diffusion-weighted magnetic resonance (MR) images. Diagnosis of probable CJD was made according to the WHO criteria [23].

Each GSS patient was from a different pedigree and had a family history of the same disease, carrying a proline-to-leucine mutation at codon 102 and methionine homozygosity at codon 129 of the PrP gene. GSS1 and GSS2, having a 9- and 20-month clinical duration from the onset, respectively, showed signs of moderate cerebellar ataxia, such as gait disturbance and slurred speech; however, they could walk unassisted and had slight or no cognitive impairment. GSS1 and GSS2 scored 22 and 26 points, respectively, on the Mini-Mental State Examination. GSS3, having a 27-month clinical duration, showed severe gait disturbance and slurred speech and was unable to walk unassisted; however, she had no cognitive impairment (30 points on the Mini-Mental State Examination) at the time of this study.

AD diagnosis was made according to the National Institute of Neurological and Communicative Diseases and Stroke-Alzheimer's Disease and Related Disorders Association (NINCDS-ADRDA) criteria [24]. CJD, GSS and AD patients were recruited from Miyagi National Hospital, Fukuoka University Hospital, Kagoshima University Hospital and Tohoku University Hospital. Normal controls were recruited from volunteers with no cognitive impairment or cerebrovascular lesions on MR images and who were not taking any centrally acting medications. No significant difference in age distribution was apparent between the groups. This study was approved by the Ethics Committee on clinical investigations of Tohoku University School of Medicine and performed in accordance with the Declaration of Helsinki. Written informed consent was obtained after complete description of the study to the patients and subjects.

Image acquisition protocols

PET scans were performed using a SET-2400W (Shimadzu Inc., Kyoto, Japan). After intravenous injection of 211–366 MBq (5.7–9.9 mCi) of [^{11}C]BF-227, dynamic PET images were obtained for 60 min with the subjects' eyes closed. Arterial blood sampling in the TSE patients was not

Table 1 Regional to pons standardized uptake value ratio (SUVRp) values in aged normal controls (Control), Alzheimer's disease patients (AD), Creutzfeldt-Jakob disease patients (CJD) and Gerstmann-Sträussler-Scheinker disease patients (GSS)

	Control (n=10) Mean ± SD	AD (n=17) Mean ± SD	CJD1	CJD2	GSS (n=3) Mean ± SD	GSS1	GSS2	GSS3
Frontal	0.60±0.03	0.64±0.04	0.57	0.61	0.67±0.08	0.74	0.69	0.57
Lateral temporal	0.59±0.03	0.69±0.04*	0.63	0.62	0.67±0.05*	0.71	0.68	0.61
Parietal	0.62±0.02	0.69±0.04*	0.62	0.62	0.67±0.06	0.72	0.68	0.61
Occipital	0.62±0.04	0.65±0.05	0.62	0.69	0.67±0.07	0.74	0.67	0.60
Medial temporal	0.64±0.04	0.62±0.03	0.57	0.65	0.67±0.02**	0.66	0.70	0.67
Striatum	0.71±0.04	0.75±0.04*	0.69	0.72	0.76±0.04	0.80	0.77	0.72
Thalamus	1.00±0.04	1.01±0.04	0.97	1.04	1.08±0.00*, **	1.08	1.07	1.08
Cerebellum	0.58±0.01	0.57±0.02	0.58	0.59	0.62±0.01*, **	0.61	0.63	0.61

*p<0.05 compared to aged normal group

**p < 0.05 compared to AD group

performed because the Committee on Clinical Investigation at Tohoku University School of Medicine did not approve blood sampling during the PET scan, from the standpoint of infection risk management. T_1-weighted MR images were obtained using a Signa 1.5-T machine (General Electric Inc., Milwaukee, WI, USA).

Image analysis

Standardized uptake value (SUV) images of [^{11}C]BF-227 were obtained by normalizing tissue concentration by injected dose and body weight. Average summations of SUV images were created from early frames (0–30 min post-injection) and late frames (40–60 min post-injection) of dynamic PET images. Early frame images were created for co-registration with individual MR images, and late frame images were used for calculation of SUV. Individual MR images were anatomically co-registered with the early frame PET images using statistical parametric mapping software (SPM2, Welcome Department of Imaging Neuroscience, London, UK) [25]. Spatial normalization was performed using an MR T_1 template of SPM2 to transfer PET images into a standard stereotactic space. Regions of interest (ROIs) were placed on a spatially normalized MR image, as described previously [12]. ROI information was then copied onto delayed PET SUV images, and regional SUV images at 40–60 min post-injection were sampled using Dr.View/LINUX software (AJS, Tokyo, Japan). Deposition of PrP plaques is reportedly frequent in the cerebellum but scarce in the pons of GSS brain [26]. Furthermore, BF-227 retention in the pons does not differ between AD patients and normal controls. Therefore, we used the pons as a reference region and calculated the regional to pons SUV ratio (SUVRp) as an index of BF-227 retention.

Statistical analysis

For statistical comparison in each group, we applied one-way analysis of variance, followed by the Bonferroni-Dunn post hoc test. Statistical comparison of age distribution was performed using the Kruskal-Wallis test, followed by Dunn's multiple comparison test. Statistical significance for each analysis was defined as $p<0.05$.

Results

Autoradiography examination indicated binding of a tracer dose of BF-227 to PrP plaque deposits. BF-227 retention was present in brain sections from GSS cases with PrP plaque deposition but not from normal control cases and sporadic CJD cases with synaptic PrP deposition (Fig. 1a–c). The regional distribution of [^{18}F]BF-227 in the autoradiograms co-localized with the immunostained PrP plaques in the cerebellar cortex of GSS cases (Fig. 1d–e). BF-227 binding to PrP plaques was additionally examined using a microscope, because BF-227 is a fluorescent compound. Core regions of the PrP plaques were intensely stained with BF-227 (Fig. 2, arrows), indicating that BF-227 preferentially binds to the fibril-rich core of PrP amyloid plaques.

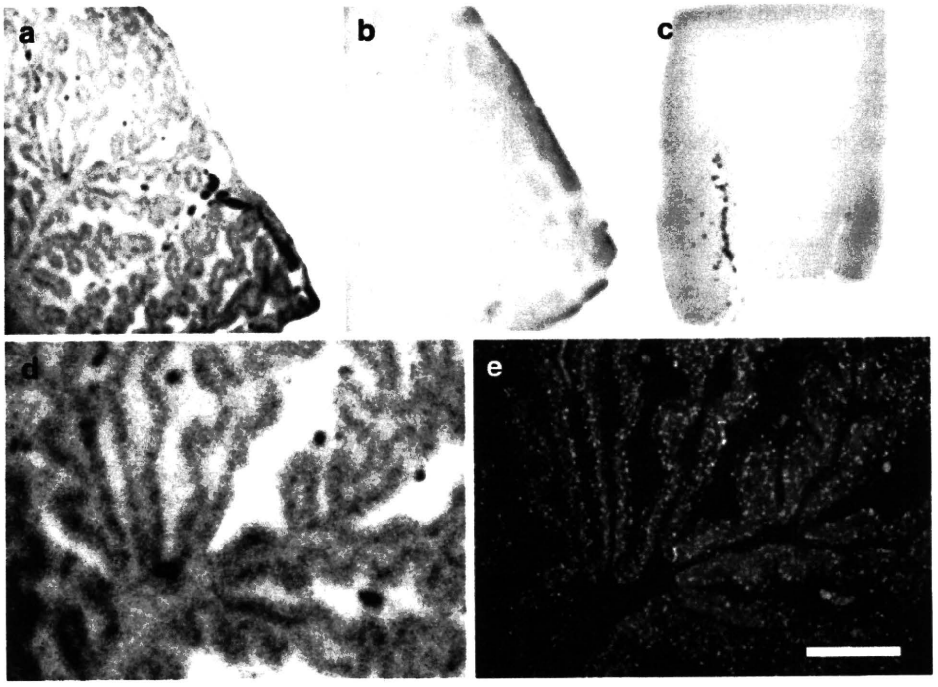

Fig. 1 [^{18}F]BF-227 autoradiograms of a cerebellar section from a Gerstmann-Sträussler-Scheinker (GSS) case (**a**), a cerebellar section from a physiological aging case (**b**) and a frontal cortex section from a sporadic Creutzfeldt-Jakob disease (CJD) case (**c**) are shown, together with a magnified view of **a** (**d**) and prion protein (PrP) immunostaining of the same field as **d** (**e**). BF-227 retention was present in the brain section from a GSS case with PrP plaque deposition, but not from a normal control case and sporadic CJD case with synaptic PrP deposition. *Bar*=200 μm

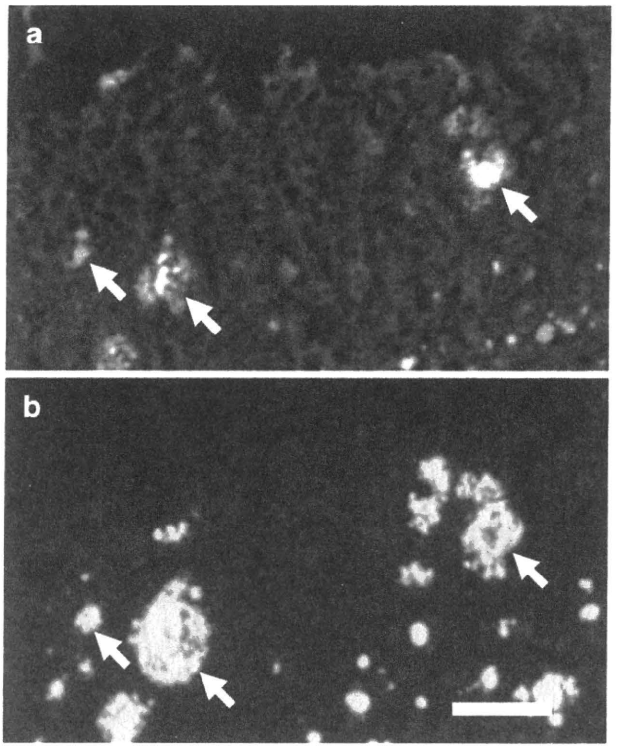

Fig. 2 Microscopic images of BF-227 staining (**a**) and PrP immunostaining (**b**) of the cerebellar cortex of a GSS case. *Arrows* indicate PrP amyloid plaques. The core regions of PrP plaques were intensely stained with BF-227. *Bar*=50 μm

Figure 3 shows the average summations of SUVRp images in an aged normal subject (64-year-old man), a sporadic CJD patient (CJD1, 63-year-old woman), a GSS patient (GSS2, 61-year-old man) and an AD patient (62-year-old woman). As reported previously, non-specific retention of [^{11}C]BF-227 was observed in the brain stem and white matter of all subjects [12]. The GSS patient showed obvious retention of [^{11}C]BF-227 in the cerebellum, and lateral and medial temporal cortices. The three GSS patients showed significantly higher SUVRp in the lateral temporal cortex, thalamus and cerebellum (Table 1, Fig. 4) when compared to aged normal controls. Furthermore, when compared to the AD group, the GSS group showed significant elevation of SUVRp in the medial temporal cortex, thalamus and cerebellum. Although two GSS patients (GSS1 and GSS2) showed retention of BF-227 in most brain regions, the youngest GSS patient (GSS3) showed BF-227 retention only in the cerebellum, thalamus and medial temporal cortex, but not in the neocortex (Table 1, Fig. 4). Furthermore, two sporadic CJD patients showed no obvious BF-227 retention in any of the brain regions examined (Table 1, Fig. 4). As previously described [12, 21], AD patients showed [^{11}C]BF-227 retention in the neocortex; however, the cerebellum and medial temporal cortex were relatively spared (Table 1).

Autopsy examination of the brain of one GSS patient (GSS1) confirmed both the presence of abundant PrP amyloid plaques in the neocortex, cerebellum, basal ganglia, thalamus, entorhinal cortex and hippocampus and the absence of Aβ amyloid plaques or other structures of misfolded protein deposition such as Lewy bodies and neurofibrillary tangles. When compared to controls, the highest SUVRp percentage difference was found in the neocortex, especially in the frontal cortex (22%), followed by the striatum (12%), thalamus (9%), cerebellum (6%) and medial temporal cortex (3%) in this case. This finding was consistent with the autopsy result showing higher density of PrP amyloid plaques in the neocortex and basal ganglia than in the cerebellum, thalamus and hippocampus. Details of clinicopathological features of this case will be published elsewhere.

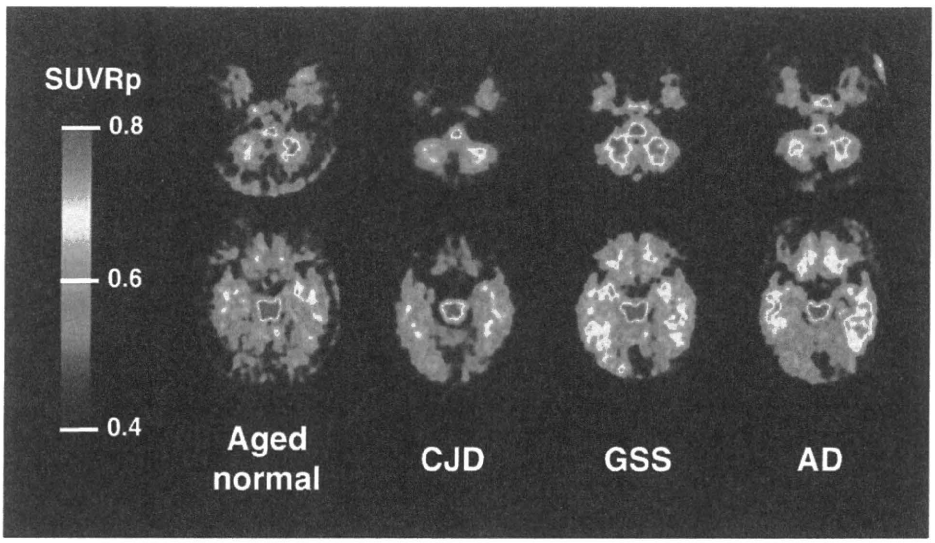

Fig. 3 Mean regional to pons standardized uptake value ratio (SUVRp) images between 40 and 60 min post-injection of [^{11}C]BF-227 in an aged normal subject (64-year-old man), a sporadic CJD patient (CJD1, 63-year-old woman), a GSS patient (GSS2, 61-year-old man) and an AD patient (62-year-old woman). Compared to the aged normal subject and CJD patient, the GSS patient showed obvious [^{11}C]BF-227 retention in the cerebellum and temporal cortex. The AD patient also showed obvious [^{11}C]BF-227 retention in the temporal cortex; however, the cerebellum was relatively spared

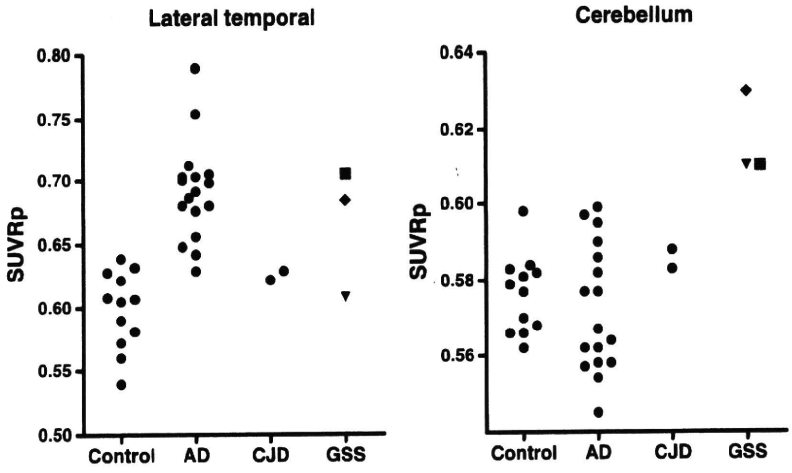

Fig. 4 SUVRp distribution in aged normal controls (*Control*), AD patients (*AD*), CJD patients (*CJD*) and GSS patients (*GSS*). GSS patients showed higher SUVRp values in the lateral temporal cortex and cerebellum. *Filled square* GSS1, *filled diamond* GSS2, *filled inverted triangle* GSS3

Discussion

This is the first study to demonstrate non-invasive detection of PrP amyloid plaques in GSS patients. GSS is neuropathologically characterized by deposits of multicentric amyloid plaques, which are especially abundant in the cerebellum, cerebral cortex and basal ganglia [3]. The present study demonstrated binding of BF-227 to PrP amyloid plaques in GSS brain sections. [^{11}C]BF-227 retention was observed in cortical and subcortical brain regions of GSS patients known for the high density of PrP plaques. Based on these findings, [^{11}C]BF-227 represents a promising candidate PET probe for the non-invasive detection of PrP amyloid plaques in the brain. However, the possibility that neocortical elevation of SUVRp in GSS patients might be caused by concomitant Aβ amyloid deposits or other misfolded protein deposits also should be considered, given that the two GSS patients showing prominent neocortical retention of [^{11}C]BF-227 were relatively older than the GSS patient showing no neocortical retention of BF-227. Although one positive GSS patient (GSS2) is still alive and was not examined neuropathologically, another positive case (GSS1) showed a high level of PrP amyloid deposits but no obvious deposits of Aβ amyloid or other misfolded proteins at autopsy. Furthermore, significant elevation of SUVRp was detected in the cerebellum, thalamus and hippocampus of all GSS cases. These brain regions are known to contain lower densities of Aβ plaques or other misfolded protein structures such as Lewy bodies. Based on these findings, it seems unlikely that concomitant deposition of Aβ amyloid or other misfolded proteins contributes to the high [^{11}C]BF-227 retention in GSS patients.

There is an increasing demand for in vivo detection of abnormal PrP deposition in the brain for the diagnosis of TSEs that might translate in early therapeutic intervention. Although GSS and other familial forms of TSEs can be diagnosed with PrP gene analysis using peripheral blood cells, it has been impossible to non-invasively measure the amount of abnormal PrP deposition in the brain. In a fashion similar to GSS, PrP amyloid deposition in the brain is commonly present in vCJD in which PrP amyloid plaques, called florid plaques, are pathognomonic [27]. Thus, [^{11}C]BF-227 PET might be a sensitive probe for the detection of PrP amyloid plaque deposition in vCJD as well as GSS, allowing longitudinal monitoring of PrP amyloid plaque deposition in the brain. Ante-mortem diagnosis of vCJD relies on the detection of abnormal PrP deposition in tonsil biopsy samples [28]. However, functional imaging using PET has an advantage over surgical biopsy tests in terms of both a non-invasive and an infection risk management point of view.

GSS is a rare form of TSE occurring in only about 3% of TSE cases in Japan. However, GSS is probably one of the TSEs most likely to benefit from early therapeutic interventions because the disease can be confirmed earlier using PrP gene analysis and progression occurs much more slowly than that in sporadic CJD, which comprises the majority of TSE cases. Recently, compounds such as pentosan polysulphate and doxycycline have been clinically used for experimental treatments for TSEs to prevent deposition of abnormal PrP in the brain, because these compounds slowed the disease progression in animal disease models when administered in an earlier stage of the disease [29–33]. Reliable surrogate markers are also required to evaluate the efficacy of these experimental interventions, and [^{11}C]BF-227 PET might be one of the best candidates to assess PrP amyloid deposition in GSS. However, it remains to be elucidated if PrP amyloid levels are a particularly relevant marker of therapeutic efficacy.

A previous PET study demonstrated moderate FDDNP retention and no remarkable PIB retention in the brain of two familial CJD patients with an octapeptide repeat insertion mutation [17]. A recent PET study has additionally demonstrated no PIB retention in two autopsy-confirmed sporadic

CJD patients [18]. In contrast with these studies, the present study successfully demonstrated prominent [^{11}C]BF-227 retention in the brain of GSS patients. Differences between the previous and present findings might mainly reside in the amount and type of PrP amyloid deposits in the brain, where histopathological studies indicate higher density of PrP amyloid plaques in GSS than in familial CJD [1]. In the present study, the findings in two sporadic CJD patients showing no obvious [^{11}C]BF-227 retention in the brain additionally support this speculation. The difference may also be attributable to higher binding affinity of BF-227 to PrP amyloid cores compared to FDDNP and PIB. To clarify this, further in vitro studies comparing the binding affinities of different amyloid tracers to PrP plaques in TSE brain homogenates are needed.

The youngest GSS patient (GSS3) showed BF-227 retention in the cerebellum and thalamus but not in the neocortex. The clinical symptoms in this patient were consistent with the brain distribution of BF-227, with the patient presenting with severe gait disturbance and slurred speech resulting from cerebellar ataxia but no signs of cognitive impairment, suggesting a close relationship between PrP plaque deposition as measured by BF-227 and regional brain dysfunction. There are variations of clinical phenotypes in GSS [1, 3]. Such variations are yet to be explained; however, the pattern of regional PrP amyloid distribution might be one of the factors affecting clinical phenotypes of GSS. In vivo PrP amyloid imaging using [^{11}C]BF-227 or other PET tracers will clarify neuropathological aspects of clinical variations in GSS.

In summary, we confirmed binding of BF-227 to PrP plaques in vitro and in vivo. A clinical PET study using [^{11}C]BF-227 demonstrated in vivo detection of PrP amyloid plaques in GSS patients. This imaging technique provides a potential means of facilitating both early diagnosis and non-invasive disease monitoring of certain forms of TSEs because, despite a lack of selectivity for PrP, brain retention of BF-227 in GSS shows a distinct pattern of regional distribution than that usually observed in sporadic AD.

Acknowledgment We appreciate the assistance of Dr. S. Watanuki, Dr. M. Miyake and Dr. H. Takashima in the clinical PET studies. This study was supported in part by the Program for the Promotion of Fundamental Studies in Health Science of the NIBIO in Japan, Industrial Technology Research Grant Program of the NEDO in Japan, and Health and Labor Sciences Research Grants (Translational Research and Research on Measures for Intractable Diseases) from the Ministry of Health, Labor, and Welfare of Japan.

References

1. DeArmond SJ, Kretzschmar HA, Prusiner SB. Prion diseases. In: Graham DI, Lantos PL, editors. Greenfield's neuropathology, 7th ed. London: Hodder Arnold. p. 273–323.
2. Collins SJ, Lawson VA, Masters CL. Transmissible spongiform encephalopathies. Lancet 2004;363:51–61.
3. Collins S, McLean CA, Masters CL. Gerstmann-Sträussler-Scheinker syndrome, fatal familial insomnia, and kuru: a review of these less common human transmissible spongiform encephalopathies. J Clin Neurosci 2001;8:387–97.
4. Noguchi-Shinohara M, Hamaguchi T, Kitamoto T, Sato T, Nakamura Y, Mizusawa H, et al. Clinical features and diagnosis of dura mater graft associated Creutzfeldt Jakob disease. Neurology 2007;69:360–7.
5. Lasmézas CI, Deslys JP, Demaimay R, Adjou KT, Hauw JJ, Dormont D. Strain specific and common pathogenic events in murine models of scrapie and bovine spongiform encephalopathy. J Gen Virol 1996;77(Pt 7):1601–9.
6. Schulz-Schaeffer WJ, Tschöke S, Kranefuss N, Dröse W, Hause-Reitner D, Giese A, et al. The paraffin-embedded tissue blot detects PrP(Sc) early in the incubation time in prion diseases. Am J Pathol 2000;156:51–6.
7. Fraser JR. What is the basis of transmissible spongiform encephalopathy induced neurodegeneration and can it be repaired? Neuropathol Appl Neurobiol 2002;28:1–11.
8. Small GW, Kepe V, Ercoli LM, Siddarth P, Bookheimer SY, Miller KJ, et al. PET of brain amyloid and tau in mild cognitive impairment. N Engl J Med 2006;355:2652–63.
9. Klunk WE, Engler H, Nordberg A, Wang Y, Blomqvist G, Holt DP, et al. Imaging brain amyloid in Alzheimer's disease with Pittsburgh Compound-B. Ann Neurol 2004;55:306–19.
10. Verhoeff NP, Wilson AA, Takeshita S, Trop L, Hussey D, Singh K, et al. In-vivo imaging of Alzheimer disease beta-amyloid with [11C]SB-13 PET. Am J Geriatr Psychiatry 2004;12:584–95.
11. Rowe CC, Ackerman U, Browne W, Mulligan R, Pike KL, O'Keefe G, et al. Imaging of amyloid beta in Alzheimer's disease with 18F-BAY94–9172, a novel PET tracer: proof of mechanism. Lancet Neurol 2008;7:129–35.
12. Kudo Y, Okamura N, Furumoto S, Tashiro M, Furukawa K, Maruyama M, et al. 2-(2-[2-Dimethylaminothiazol-5-yl]ethenyl)-6-(2-[fluoro]ethoxy)benzoxazole: a novel PET agent for in vivo detection of dense amyloid plaques in Alzheimer's disease patients. J Nucl Med 2007;48:553–61.
13. Ishikawa K, Doh-ura K, Kudo Y, Nishida N, Murakami-Kubo I, Ando Y, et al. Amyloid imaging probes are useful for detection of prion plaques and treatment of transmissible spongiform encephalopathies. J Gen Virol 2004;85:1785–90.
14. Bresjanac M, Smid LM, Vovko TD, Petric A, Barrio JR, Popovic M. Molecular-imaging probe 2-(1-[6-[(2-fluoroethyl)(methyl) amino]-2-naphthyl]ethylidene) malononitrile labels prion plaques in vitro. J Neurosci 2003;23:8029–33.
15. Sadowski M, Pankiewicz J, Scholtzova H, Tsai J, Li Y, Carp RI, et al. Targeting prion amyloid deposits in vivo. J Neuropathol Exp Neurol 2004;63:775–84.
16. Hoefert VB, Aiken JM, McKenzie D, Johnson CJ. Labeling of the scrapie-associated prion protein in vitro and in vivo. Neurosci Lett 2004;371:176–80.
17. Boxer AL, Rabinovici GD, Kepe V, Goldman J, Furst AJ, Huang SC, et al. Amyloid imaging in distinguishing atypical prion disease from Alzheimer disease. Neurology 2007;69:283–90.
18. Villemagne VL, McLean CA, Reardon K, Boyd A, Lewis V, Klug G, et al. 11C-PiB PET studies in typical sporadic Creutzfeldt-Jakob disease. J Neurol Neurosurg Psychiatry 2009;80:998–1001. doi:10.1136/jnnp.2008.171496.
19. Okamura N, Suemoto T, Shimadzu H, Suzuki M, Shiomitsu T, Akatsu H, et al. Styrylbenzoxazole derivatives for in vivo imaging of amyloid plaques in the brain. J Neurosci 2004;24:2535–41.
20. Ishikawa K, Kudo Y, Nishida N, Suemoto T, Sawada T, Iwaki T, et al. Styrylbenzoazole derivatives for imaging of prion plaques and treatment of transmissible spongiform encephalopathies. J Neurochem 2006;99:198–205.

21. Waragai M, Okamura N, Furukawa K, Tashiro M, Furumoto S, Funaki Y, et al. Comparison study of amyloid PET and voxel-based morphometry analysis in mild cognitive impairment and Alzheimer's disease. J Neurol Sci 2009;285:100–8. doi:10.1016/j.jns.2009.06.005.
22. Okamura N, Furumoto S, Funaki Y, Suemoto T, Kato M, Ishikawa Y, et al. Binding and safety profile of novel benzoxazole derivative for in vivo imaging of amyloid deposits in Alzheimer's disease. Geriatr Gerontol Int 2007;7:393–400.
23. Zeidler M, Gibbs CJ Jr, Meslin F. WHO manual for strengthening diagnosis and surveillance of Creutzfeldt-Jakob disease. Geneva: World Health Organization; 1998. p. 47–51.
24. McKhann G, Drachman D, Folstein M, Katzman R, Price D, Stadlan EM. Clinical diagnosis of Alzheimer's disease: report of the NINCDS-ADRDA Work Group under the auspices of Department of Health and Human Services Task Force on Alzheimer's Disease. Neurology 1984;34:939–44.
25. Friston KJ, Holmes AP, Worsley KJ, Poline JP, Frith CD, Frackowiack RSJ. Statistical parametric maps in functional imaging: a general linear approach. Hum Brain Mapp 1995;2:189–210.
26. Masters CL, Gajdusek DC, Gibbs CJ Jr. Creutzfeldt-Jakob disease virus isolations from the Gerstmann-Sträussler syndrome with an analysis of the various forms of amyloid plaque deposition in the virus-induced spongiform encephalopathies. Brain 1981;104:559–88.
27. Ironside JW, McCardle L, Horsburgh A, Lim Z, Head MW. Pathological diagnosis of variant Creutzfeldt-Jakob disease. APMIS 2002;110:79–87.
28. Hill AF, Zeidler M, Ironside J, Collinge J. Diagnosis of new variant Creutzfeldt-Jakob disease by tonsil biopsy. Lancet 1997;349:99–100.
29. Doh-ura K, Ishikawa K, Murakami-Kubo I, Sasaki K, Mohri S, Race R, et al. Treatment of transmissible spongiform encephalopathy by intraventricular drug infusion in animal models. J Virol 2004;78:4999–5006.
30. Rainov NG, Tsuboi Y, Krolak-Salmon P, Vighetto A, Doh-Ura K. Experimental treatments for human transmissible spongiform encephalopathies: is there a role for pentosan polysulfate? Expert Opin Biol Ther 2007;7:713–26.
31. De Luigi A, Colombo L, Diomede L, Capobianco R, Mangieri M, Miccolo C, et al. The efficacy of tetracyclines in peripheral and intracerebral prion infection. PLoS One 2008;3:e1888.
32. Teruya K, Kawagoe K, Kimura T, Chen CJ, Sakasegawa Y, Doh-ura K. Amyloidophilic compounds for prion diseases. Infect Disord Drug Targets 2009;9:15–22.
33. Forloni G, Salmona M, Marcon G, Tagliavini F. Tetracyclines and prion infectivity. Infect Disord Drug Targets 2009;9:23–30.

FEBS Letters 584 (2010) 1193–1198

ELSEVIER

FEBS Letters

journal homepage: www.FEBSLetters.org

GABAA receptor subunit β1 is involved in the formation of protease-resistant prion protein in prion-infected neuroblastoma cells

Tomohiro Kimura [a], Kensuke Ishikawa [a,1], Yuji Sakasegawa [a], Kenta Teruya [a], Tetsutaro Sata [b], Hermann Schätzl [c], Katsumi Doh-ura [a,*]

[a] Department of Prion Research, Tohoku University Graduate School of Medicine, Sendai, Japan
[b] Department of Pathology, National Institute of Infectious Diseases, Toyama 1-23-1, Shinjuku, Tokyo 162-8640, Japan
[c] Institute of Virology, Prion Research Group, Technische Universität München, Trogerstr. 30, 81675 Munich, Germany

ARTICLE INFO

Article history:
Received 25 December 2009
Revised 5 February 2010
Accepted 11 February 2010
Available online 14 February 2010

Edited by Jesus Avila

Keywords:
Prion
GABAA receptor
gabrb1
siRNA
Antagonist

ABSTRACT

γ-Aminobutyric acid type A (GABAA) receptor β1 (gabrb1), a subunit of GABAA receptors involved in inhibitory effects on neurotransmission, was found to associate with the formation of protease-resistant prion protein in prion-infected neuroblastoma cells. Silencing of gabrb1 gene expression significantly decreased the abnormal prion protein level but paradoxically increased the normal prion protein level. Treatment with a gabrb1-specific inhibitor, salicylidene salicylhydrazide, dose-dependently decreased the abnormal prion protein level, but silencing of other GABAA receptor subunits' gene expression and treatments with the receptor antagonists and agonists did not. Therefore, gabrb1 involvement in abnormal prion protein formation is independent of GABAA receptors.

1. Introduction

Transmissible spongiform encephalopathies or prion diseases are fatal neurodegenerative disorders that include Creuzfeldt–Jakob disease in humans, and bovine spongiform encephalopathy and scrapie in animals. These diseases are characterized by deposition of a partially protease-resistant abnormal isoform of prion protein (PrPres), which is the main component of the pathogen and which is converted from the normal cellular isoform of prion protein (PrPc) in the central nervous system and lymphoreticular system [1]. Cell biology of the biosynthesis and metabolism of PrPc and PrPres has been eagerly investigated in prion-infected cells [2,3] but has not been fully elucidated. Especially, endogenous factors involved in the formation of PrPres or the conformational change from PrPc into PrPres [4,5] remain enigmatic.

Using gene screening by the gene silencing technique with small interfering RNA (siRNA) or short hairpin RNA (shRNA) [6,7], we have sought endogenous factors affecting the metabolism of PrPres in prion-infected neuroblastoma cells. We report here a possible linkage of γ-aminobutyric acid A receptor β1 (gabrb1) with the formation of PrPres. In fact, gabrb1 is a subunit of γ-aminobutyric acid type A (GABAA) receptors responsible for most of the fast inhibitory synaptic transmission in mammalian brain [8]. Belonging to the ligand-gated ion channels, they are formed by the pentameric assembly of homologous subunits. Numerous GABAA receptor subunits have been identified (α1–6, β1–3, γ1–3, δ, π, ε, and θ), all of which are products of separate genes, and most GABAA receptors contain two α subunits, two β subunits and either one γ subunit or one δ subunit [8]. It has been well documented that GABAergic neurons are affected by prion infection [9–15], but it is not clear whether GABAA receptors are involved in PrPres formation. Therefore, to address this query, we performed gene silencing experiments for gabrb1 and other representative GABAA receptor subunits (α5, β3, γ2, and δ) as well as GABAA receptor modulating experiments using the antagonists and agonists in prion-infected cells.

2. Materials and methods

2.1. siRNAs and compounds

Double-stranded siRNAs for GABAA receptor subunits used for this study (Table 1) were purchased from Invitrogen Corp. (Carlsbad, CA, USA). Some GABAA receptor antagonists (bicuculline

* Corresponding author. Address: Department of Prion Research, Tohoku University Graduate School of Medicine, 2-1 Seiryo-machi, Aoba-ku, Sendai 980-8575, Japan. Fax: +81 22 717 7656.
E-mail address: doh-ura@mail.tains.tohoku.ac.jp (K. Doh-ura).
[1] Present address: Department of Psychiatry, Saga University School of Medicine, Saga, Japan.

0014-5793/$36.00 © 2010 Federation of European Biochemical Societies. Published by Elsevier B.V. All rights reserved.
doi:10.1016/j.febslet.2010.02.029

methiodide and picrotoxin) and agonists (GABA, muscimol, and isoguvacine hydrochloride) were purchased from Sigma–Aldrich Corp. (St. Louis, MO, USA). Another agonist, pentobarbital, was purchased as a 5% (approximately 200 mM) solution of its sodium salt, nembutal, from Dainippon Sumitomo Pharma Co. Ltd. (Osaka, Japan). A specific inhibitor of GABAA receptor β1 subunit, salicylidene salicylhydrazide, was obtained from Tocris Bioscience (Missouri, USA).

2.2. shRNA expression vectors

The DNA fragments flanking 5′ *Bam*HI recognition sequence and 3′ *Hind*III recognition sequence, which corresponded to shRNA sequences for GABAA receptor subunits, were produced by annealing pairs of sense and antisense 64mer oligonucleotides, of which sense sequences were designed as follows: 5′-GATCC***GAg-GGTGGAGTTCAtAAtAGG***CTTCCTGTCA***CCTGTTGTGAACTCCACCTTC***-TTTTTTA-3′ targeting to nucleotides 663–683 of β1 subunit coding sequence; 5′-GATCC***ACCTGGTgTGAtAGAtGTTTG***CTTCCTGTCA***CAA-ACGTCTGTCATACCAGGT***TTTTTTA-3′ targeting to nucleotides 355–375 of γ2 subunit coding sequence; 5′-GATCC***GAATGGGCTgCTT-tACtATCC***CTTCCTGTCA***GGATGGTGAAGTAGCCCATTC***TTTTTTA-3′ targeting to nucleotides 809–829 of γ2 subunit coding sequence; 5′-GATCC***ACATGGAgTACACtATGAtTG***CTTCCTGTCA***CAGTCATGGTG-ATTTCCATGT***TTTTTTA-3′ targeting to nucleotides 245–265 of δ subunit coding sequence. Bold italic letters and small bold italic letters, respectively denote target sites and mismatch-induced sites. The DNA fragments were ligated into a pBAsi-hH1 (Takara Bio Inc., Shiga, Japan) cut with *Bam*HI and *Hind*III. The ligated vectors were introduced into *Escherichia coli*; then plasmids of interest were harvested and sequenced.

2.3. Mutated gabrb1 expression vector

Mouse gabrb1 gene was cloned from a ready mouse brain cDNA library (Marathon; Takara Bio Inc.) using PCR with KOD-plus DNA polymerase (Toyobo Co. Ltd., Osaka, Japan). A PCR product was inserted into a pcDNA3.1 Myc/His expression vector (Invitrogen Corp.). The ligated vectors were introduced into *E. coli*; then plasmids of interest were harvested and sequenced. Mutations were induced by site-directed mutagenesis using PCR technique with primers of 5′-GATGCATCTGCAGCgcGtGTgGCtCTtGGtATaACaAC-GGTGCTG-3′ (small italic letters indicate silent mutations induced) and 5′-TGCAGATGCATCATAGTTGATCCA-3′. The PCR products were treated with *Dpn*I for digesting template plasmids and introduced directly into *E. coli*; then plasmids of interest were harvested and sequenced.

2.4. Gene silencing experiments

Mouse neuroblastoma N2a cells infected persistently with RML prion strain (ScN2a) or 22L prion strain (N167) were diluted to 10% or 15% confluence with Opti MEM I (Invitrogen Corp.) including 10% fetal bovine serum (FBS), and 2.4 ml each was seeded onto six-well plates. Transfection was performed on the next day of seeding. TransFectin (3.0 μl/well; Bio-Rad Laboratories, Inc., Hercules, CA, USA) was used for the transfection of shRNA expression vectors, and siLentFect (3.0 μl/well, Bio-Rad Laboratories, Inc.) was used for transfection of double-stranded siRNAs. The amounts of vectors or siRNAs used in transfection were, respectively, 0.2 μg per well or 20 nM per well. Medium was changed on the day after transfection. Cells were harvested after washing with PBS 3 days after transfection.

Table 1
siRNAs and shRNAs used for this study.

GABAA receptor subunit examined	Nucleotide position of target region*	
	siRNA (catalog no.**)	shRNA
α5	311–335 (MSS201426)	
β1	820–844 (MSS204523)	663–683
β3	873–897 (MSS204527)	
β3 transcript variant 1	62–86 (MSS204528)	
γ2		355–375, 809–829
δ		245–265

* Nucleotide position in the coding sequence of each GABAA receptor subunit gene.
** siRNAs were obtained from Invitrogen Corp. (Carlsbad, CA, USA).

2.5. Rescue experiment

The ScN2a cells were diluted to 15% confluence with Opti MEM I including 10% FBS, and 2 ml each was seeded onto six-well plates. Transfection was performed on the day after seeding. TransFectin (2.0 μl/well) was used for the transfection of both mutated gabrb1 expression vector and double-stranded siRNA. The amounts of the vector and the siRNA used for transfection were, respectively, 0.8 μg per well and 5 nM per well. Medium was changed on the day after transfection. Cells were harvested after washing with PBS 3 days after transfection.

2.6. Immunoblotting

Cells were lysed with lysis buffer (0.5% sodium deoxycholate, 0.5% Nonidet P-40, PBS) after rinsed with PBS, and debris was eliminated by centrifugation at 3000×*g* for 10 min at 4 °C. Protein contents of each sample were measured using a modified Lowry method [16] with Dc protein assay reagent (Bio-Rad Laboratories, Inc.) with bovine serum albumin as a standard. For PrPres detection, cell lysate containing the same protein amount was treated with 10 μg/ml of proteinase K for 30 min at 37 °C, and PrPres was pelleted by centrifugation at 20 000×*g* for 20 min at 4 °C. After denaturation in sample buffer by heating at 95 °C for 10 min, PrP was separated using SDS–PAGE and then transferred onto Immobilon-P membrane (Millipore Corp., Bedford, MA, USA). Subsequently, PrP was detected using a monoclonal antibody SAF83 as a primary antibody, which recognizes residues 126–164 of mouse PrP (1:5000; SPI-Bio, Massy, France), and an alkaline phosphatase-conjugated goat anti-mouse antibody (1:20 000; Promega Corp., Madison, WI, USA) as a secondary antibody. Immunoreactivity was visualized using CDP-Star detection reagent (Amersham, Piscataway, NJ, USA) and was analyzed densitometrically using the ImageJ program (National Institutes of Health, Bethesda, MD, USA). To check the sample integrity, protein levels of GAPDH and β-actin were analyzed in the same samples used for PrPres detection.

2.7. Quantification of mRNA level

Cells were lysed with RNAiso-plus reagent (Takara Bio Inc.). Total RNA was extracted using FastPure RNA (Takara Bio Inc.). Poly A^+ RNA was purified from total RNA using an isolation kit (MicroFast Track MAG micro mRNA; Invitrogen Corp.). In addition, cDNA was synthesized with first strand cDNA synthesis kit (Takara Bio Inc.). The mRNA level was measured by real-time PCR using SYBR Premix Ex Taq II (Takara Bio Inc.) or using TaqMan probe with gene expression assay master mix for gabrb1 (Mm00433461_m1; Applied Biosystems). Fold change of gene expression was calculated using the $2^{-\Delta\Delta Ct}$ method, with GAPDH as an internal control.

2.8. Statistical analyses

Statistical significance was analyzed using one-way analysis of variance followed by the Tukey–Kramer post-hoc test for multiple

sample comparisons, or using a *t*-test for the two sample comparisons. Statistical significance for each analysis was defined as $P < 0.05$.

3. Results

3.1. Effects of gabrb1 gene silencing

Gene silencing of gabrb1 in ScN2a cells by transfection of shRNA expression vector targeting at nucleotides 663–683 of gabrb1 coding sequence demonstrated a significant decrease in both gabrb1 mRNA level (Fig. 1a) and PrPres formation (Fig. 1b). On the other hand, the PrP mRNA level increased significantly (Fig. 1a); upregulation in PrPc protein level was confirmed in uninfected N2a cells as well as ScN2a cells (Fig. 1a and c). Similar results were also observed in the gene silencing experiment using double-stranded siRNA, which was designed to target at nucleotides 820–844 of gabrb1 coding sequence (Fig. 1d–f). Protein levels of GAPDH and β-actin in the cells treated with the gabrb1 shRNA or siRNA were consistent with those of the mock controls (Fig. 1b and e), indicating that the reduction of PrPres level was not attributable to either sample preparation artifacts or cell viability difference. On the other hand, in comparison with ScN2a cells, N167 cells showed a less remarkable decrease in PrPres formation when treated with the gabrb1 siRNA (Supplementary Fig. 1).

Other representative subunits of GABAA receptor, including β3 and one of its transcript variants, as well as α5, γ2, and δ, were subjected to gene silencing experiments in ScN2a cells, but no modification in the PrPres level was observed despite marked reduction in mRNA levels of the target genes (Supplementary Fig. 2). These subunits were chosen from the following facts. Most GABAA receptors contain two α subunits, two β subunits, and either one γ subunit or one δ subunit [8]. The α5 subunit is reportedly upregulated in the brain when prion is inoculated into the mice expressing anchorless PrP [17]. The β3 subunit is the most abundant β subunit observed in ScN2a (data not shown). The γ2 subunit is the most abundant subunit in the brain and is incorporated in most GABAA receptor subtypes [18]. The δ subunit comprises only one member. In addition to the subunits described, the β2 subunit was also examined in this study, but its gene silenc-

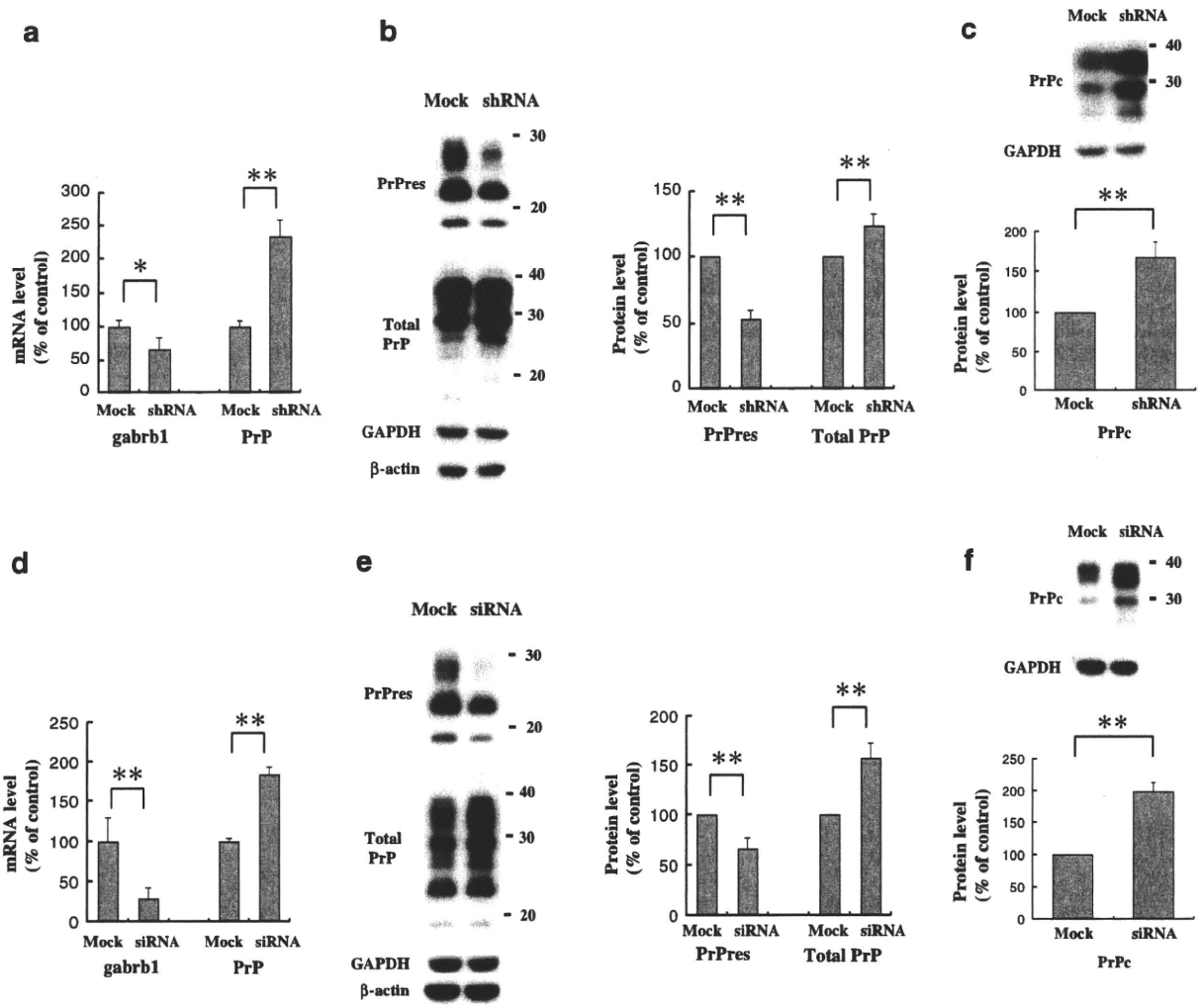

Fig. 1. Effects of gabrb1 gene silencing. Data from ScN2a cells transfected with shRNA expression vector or mock vector are shown: mRNA level of gabrb1 and PrP (a); immunoblot and protein level of PrPres and total PrP (b). Immunoblot and protein level of PrPc from N2a cells transfected with shRNA expression vector or mock vector are shown in (c). Data from ScN2a cells transfected with double-stranded siRNA or transfection reagent only (mock) are shown: immunoblot and protein level of PrPres and total PrP (d); mRNA level of gabrb1 and PrP (e). Immunoblot and protein level of PrPc from N2a cells transfected with double-stranded siRNA or transfection reagent only (mock) are shown in (f). Molecular size markers in the right side of the immunoblots are shown in kilodaltons. Immunoblot data shown here are representative examples; the graphic data shown here are the average and standard deviation from results of independent triplicate experiments (*$P < 0.05$, **$P < 0.01$).